COO-7-6304

Differential Cross Sections for Small Angle Scattering of 24-MeV Neutrons by Protons

T.G. Masterson[†]

University of Wisconsin, Madison, Wisconsin[††]

ABSTRACT

Absolute n-p elastic scattering cross sections were measured at 19.5° and 25.1° (lab) for an incident neutron energy of 24 MeV. A liquid scintillator detected both the incident and scattered neutrons. The scatterer was a liquid scintillator also. The c.m. differential cross sections were 31.3±0.5 and 30.7±0.6 mb/sr at c.m. scattering angles of 39.3° and 50.5°, respectively. The present results agree with the cross sections predicted by Hopkins and Breit.

DISCLAIMER

I. INTRODUCTION

An accurate knowledge of n-p differential cross sections tests our understanding of the nucleon-nucleon interaction and is needed for the measurement of fast neutron flux. In 1957 Gammel[1] proposed an energy dependent fit to the available data of the form $A(1 + B \cos^2\Theta_{c.m.})$ for energies below 42 MeV. Later data[2] have shown that the interaction is not symmetric about 90° in the c.m. system indicating the need for a cos Θ term. Recently, Hopkins and Breit[3] have used the Yale and LRL nucleon-nucleon phase shift analyses to obtain fourth order Legendre polynomial expansions for the differential cross section. They predict that the coefficients of the P_1 and P_2 terms have approximately the same magnitude between 20 and 30 MeV. At 24 MeV, the anisotropy in the cross section reaches 10%, and the P_1 and P_2 terms account for most of this anisotropy.

Most measurements of the differential cross section have used a counter telescope for detecting recoil protons, but this method does not work at forward angles because of the small recoil proton energy. The most accurate measurements near 24 MeV are by Rothenberg[4] and Burrows[5] who has extended the range of this method down to a c.m. scattering angle of about 70°. These measurements are all relative and must be normalized to the total cross section. This normalization requires a knowledge of the scattering at small angles where the cross section is not well known.

The only previous forward angle scattering measurement was by the Harwell group[2] and their energy resolution was poor (fwhm of 5 MeV).

The present paper reports an absolute measurement of the differential scattering cross section at 19.5 and 25.1°(lab). Both the intensity of neutrons scattered through an angle θ by a target scintillator and the intensity of the incident 0° neutron beam (see Fig. 1a, b) were measured. The use of the same detector for both measurements made an absolute determination of the incident flux density unnecessary. Only the relative efficiencies[6] of the detector for neutrons before and after scattering had to be known to normalize the number of neutrons detected at θ to the number incident on the target. The present data provide a measurement of the differential cross section at 39.3° and 50.5° (c.m.). These results may be combined with the relative measurements in the backward hemisphere (such as those by Rothenberg[4] and Burrows[5]) and with the well known total cross section to give an angular distribution.

II. EXPERIMENTAL METHOD

A. General

Neutrons of 24 MeV lab energy were incident on a target scintillator. The neutrons scattered through an angle θ pass into a detecting scintillator. The target was a liquid hydrocarbon scintillator so that the background could be reduced by requiring fast coincidences between the recoil protons of the target and the detector scintillators. The 0° neutron flux density was also measured with the detector. The count rate of neutrons observed at 0° depends on the incident flux and the detector efficiency for 24-MeV neutrons. The count rate of neutrons observed at the lab scattering angle θ depends on the same incident flux,

the n-p differential cross section and the efficiency of the detector for neutrons of energy $E_0 \cos^2\theta$. The ratio of these two count rates gives the differential cross section and is independent of the value of the incident neutron flux. The resulting cross section depends only on the ratio of the detector efficiencies at two nearby energies.

B. Neutron Source

The neutron source was the $T(d,n)^4He$ reaction. Deuterons of 7.0 MeV energy from a tandem accelerator were incident on a tritium gas cell. Figure 1c shows an expanded view of the tritium cell. The cell was 3.8 cm long and contained about 20 Ci of tritium when filled to 1 atm. Gas pressures ranged from 0.8 to 1.8 atm. Entrance and exit foils were 2.5 μm molybdenum and were changed every other day on the accelerator. Beam collimators prevented deuterons from hitting the tantalum washers which supported the molybdenum foils. The cell had an evacuated backstop and was air cooled to minimize beam heating effects. This design insured that the neutron flux density was the same for all runs. Had the deuteron beam stopped in the tritium cell, heating effects would have changed the local tritium pressure and consequently the neutron source strength. The backstop was larger in diameter than the gas cell to prevent attenuation of the neutron beam by the walls of the backstop in the ±3° range about the 0° direction. A 0.5-mm gold foil stopped the deuteron beam. It was replaced periodically to reduce the number of neutrons produced by the $D(d,n)^3He$ reaction.

The mean deuteron energy at the center of the tritium cell was 6.84 MeV (for ~ 1 atm T_2 pressure). This resulted in approximately 1.6×10^7 neutrons sr^{-1} μC^{-1} at 0° with an energy of 24.03±0.08 MeV.

C. Apparatus

Figures 1a,b show the apparatus and geometry used. The scattering target and the detector were scintillators mounted on RCA 8575 and Amperex XP1021 photomultiplier tubes, respectively. They were mounted to allow adjustment in the plane perpendicular to the beam.

Both target and detector had lucite caps with a 0.4 mm diam rod sticking up through the center. This rod defined the center of each scintillator. Distances between scintillators and gas cell were measured to ±0.2 mm.

The target was a 2.5 cm diam × 2.5 cm high NE 218 liquid scintillator[7] in a glass cylinder wrapped in aluminum foil and mounted on an RCA 8575 phototube with its axis perpendicular to the beam direction. The mass[7] of the scintillator liquid was 11.37 gm and the H/C ratio[8] was 1.28. The total number of hydrogen atoms in the sample was $(0.659\pm0.003) \times 10^{24}$.

The detector was a 2.5 cm diam by 5.1 cm high NE 218 liquid scintillator.

D. Electronics

(i) Phototube stabilization. The count rate in the target scintillator was just under 1 MHz. A Zener diode string and capacitor bank stabilized the voltage at each of the last four dynodes and increased the current handling capacity of the bleeder string. The string was air cooled and operated at about 5 mA. With the diode string in operation, no change in the pulse height spectrum of a ^{60}Co source was observed for count rates up to 5 MHz.

(ii) Electronics for data acquisition. The electronics provided recoil proton pulse height spectra for neutrons scattered from the target scintillator into the detector scintillator. Figure 2a is a simplified block diagram of the electronics. Neutrons were detected in both target and detector, and a fast (time-of-flight) coincidence requirement reduced background. A pulse shape discrimination system rejected gamma ray pulses from the detector. Figure 2b is a diagram of the actual electronics used.

E. Procedures for Taking Data

The beam current was usually between 1 and 2 μA, the lower limit determined by count rate considerations (0.5 counts/sec) and the upper limit by the maximum allowable beam on the molybdenum windows. The maximum safe current for nickel foils[9] was assumed for molybdenum.

The angular distribution of the neutron flux near 0° was measured. It varied by less than 2% over the area of the target scintillator. The data analysis took into account these deviations.

A current integrator measured the charge incident on the tritium gas cell. The calibration and zero point of the current integrator were checked at the beginning of each accelerator running period. The offset current measured with no beam on the target was less than 0.2% of the target current. A correction for this offset current was applied.

Both maximal and minimal (shadow) shielding were tried in an attempt to reduce background. Foreground/background ratios were approximately the same in each case. Observed backgrounds were about 8% at

25.1°, 28% at 19.5°. Shadow shielding was used because it was easily removable for 0° normalization runs. (See steps 1 and 4 below.) The shadow shield consisted of 30 cm iron plus 5 cm lead in the direct path of neutrons from the gas cell to the detector. (See Fig. 1b.)

The following procedure was used in taking data:

(1) Measurement of 0° neutron flux. A 0° normalization run in the direct neutron beam was taken with the detector far enough away (142 cm) from the neutron source that the count rate was less than 1 kHz. The count rate was reduced by moving the detector away from the neutron source rather than by decreasing the beam current so that the neutron source strength would be the same for this run as for each of the following runs (2)-(4). This procedure also eliminated any residual effects due to heating of the tritium cell since the deuteron current was the same for all runs.

(2) Background measurement. A 41-cm long iron shadow bar was inserted between the gas cell and the detector for a 0° background run. Typical recoil proton spectra from steps (1) and (2) are shown in Fig. 3a.

(3) Scattering data. The detector was positioned at the scattering angle θ, and the target scintillator was raised into the direct neutron beam. A time-of-flight (TOF) coincidence requirement between target and detecting scintillators was imposed, and data were collected for about 1 hour (5000 μC). A TOF spectrum of particles scattered by the target scintillator and observed in the detecting scintillator is shown in Fig. 4. These particles satisfy a fast coincidence requirement and the requirement that the particle seen in the detecting scintillator be a neutron. A 'real' neutron is a neutron which satisfies these

requirements. One channel of the TOF spectrum of 'real' neutrons is approximately 0.2ns and the fwhm of the timing spectrum is about 2ns. A simultaneously measured 'accidental' TOF spectrum is also shown on the same figure. 'Accidental' means that the particle seen in the detecting scintillator was a neutron which did not meet the flight time requirements. The 'accidental' spectrum was obtained by delaying one side of the coincidence system by about 15 ns. This delay has been removed in the figure for comparison purposes. The effect of the slight differences in the length of time for which the real and accidental coincidence gates were open was included in the data analysis.

A typical 'real' recoil proton spectrum observed at a scattering angle of 25.1° is shown in Fig. 3b. This spectrum shows the pulse height distribution of recoil protons produced by 'real' neutrons and is gated by the same logic as the 'real' TOF spectrum as indicated by the electronics shown in Fig. 2b. The numbers above the arrows indicate the bias energy expressed as a fraction of the incident neutron energy. The location of the arrows takes into account the non-linear response of the scintillator which was measured in a separate experiment.[6] An 'accidental' spectrum was measured simultaneously. It was gated by the same logic as the 'accidental' TOF spectrum.

Figure 3c shows spectra obtained at a scattering angle of 19.5°. Since the background is three times higher here, the present method has limited usefulness at smaller angles.

(4) Scattering data background. An iron shadow bar was inserted between target and detector (the shadow shielding between gas cell and detector remained in place) for a background run. All shielding

was then removed, the target scintillator was lowered out of the 0° neutron beam, and the detecting scintillator was moved to its 0° location for another 0° flux measurement.

3. THEORY AND ANALYSIS

The differential cross section for neutrons scattered by protons through a lab angle θ is[10]

$$\sigma(\theta) = \frac{s^2 d^2}{d_0^2} \frac{f_B(E_0)}{f_B(E_1)} \frac{\sigma_{np}(E_0)}{\sigma_{np}(E_1)} \frac{1}{n_p} \frac{A_\theta}{B_0} , \qquad (1)$$

where

s = distance from neutron source to target scintillator,

d = distance from target scintillator to detecting scintillator,

d_0 = distance from neutron source to detecting scintillator for 0° measurements,

$\sigma_{np}(E)$ = the n-p total cross section at energy E,

n_p = the total number of protons in the target,

A_θ = number of neutrons detected per unit charge after being scattered from the target into the detector,

B_0 = number of neutrons detected per unit charge in the 0° position, and

f_B = fraction of the total number of recoil protons detected at a given bias.

The bias factor f_B is given by

$$f_B = \int_{\Psi_{min}}^{\pi} \sigma_{c.m.}(\Psi) (\sin \Psi) d\Psi \Big/ \int_0^{\pi} \sigma_{c.m.}(\Psi) (\sin \Psi) d\Psi , \qquad (2)$$

where Ψ is the c.m. scattering angle and Ψ_{min} is the neutron scattering angle at which the recoil proton energy is equal to the bias energy B. The c.m. differential cross section is $\sigma_{c.m.}(\Psi)$ and the integral is over a differential volume element inside the detector. Table I gives values of the ratio $f_B(E_0)/f_B(E_1)$ as a function of bias energy for various assumed angular distributions. The table indicates that for these angles and biases the assumed angular distribution has little effect on the determination of the differential cross section. The Hopkins and Breit angular distribution derived from the Yale phase shifts was used in this calculation.

The lab cross sections were converted to the c.m. system using the relativistic kinematics program RELKIN.[11]

Not yet included in the relation (1) are the effects of multiple scattering, exponential attenuation, and wall effects. These will be discussed in section 4.

A computer program analyzed all recoil proton pulse height spectra and calculated a laboratory differential cross section. It took into account backgrounds, accidental coincidences, bias effects and the nonlinear response of the scintillator. It also included the effects of transmissions through shadow bars, differences in widths of TAC spectra, dead time, ADC and current integrator corrections. In addition, the program calculated statistical errors.

4. CORRECTIONS

A. Multiple Scattering.

Consider neutrons which have scattered once from a hydrogen

atom in the target scintillator through an angle θ towards the detector. The number of neutrons going in this direction may be decreased by collisions with either hydrogen or carbon atoms in their paths while leaving the target scintillator. This is called exponential attenuation of the outgoing beam or outscattering. The number of neutrons headed towards the detector may be increased by neutrons which have scattered previously from hydrogen atoms in a direction away from the detector and then scatter from either H or C towards the detector. The scattered flux may also be increased by neutrons which have scattered previously from carbon in any direction and then from hydrogen towards the detector. Neutrons interacting only with carbon are not included because carbon recoils are not detected in the target scintillator since the bias level on the target scintillator was set above the maximum light output for both carbon recoils and alpha-particles from reactions in carbon.

A Monte-Carlo computer program traced the trajectories of about 6×10^5 interacting neutrons through the target scintillator and calculated the numbers of all possible inscattering and outscattering collisions. At 25.1°, 5.5% of the detected particles were due to inscattering while 9.0% had been outscattered for a net correction of +3.4%. At 19.5°, inscattering was 2.8%, outscattering was 8.7% and the correction to the scattered flux was +5.8%.

B. Finite Geometry

The tritium gas cell is actually a neutron source of finite length and not a point source. Neutrons are assumed to be produced uniformly over this length. Thus the front of this cell subtends a

different solid angle at the target than the back of the cell. The average count rate $\bar{A}_\theta$ may be written as[10]

$$\bar{A}_\theta = A_\theta \frac{1}{1-(L/2s)^2}$$

where L is the length of the tritium gas cell and s is the distance from the center of the gas cell to the center of the target. For L = 3.8 cm and s = 34.5 cm this represents a correction of -0.3% to the differential cross section. This correction is negligible when the detector is at 0°, since the distance to the detector is about 142 cm.

The same correction may also be made for the finite length of the target. Here the differential cross section must be multiplied by the factor $1-(D/2d)^2 = 0.999$ (where the target diameter D is 2.54 cm and d is 33.4 cm) for a correction of -0.1%.

C. Attenuation in Detector

The flux actually measured in the detecting scintillator is not uniform throughout the scintillator but is exponentially attenuated along its path through the scintillator by collisions of the neutrons with C and H nuclei.

By performing an integration over the volume of the scintillator[10] we find, for an incident energy of 24 MeV, 92.3% of the incident neutrons are transmitted through the scintillator. At a scattering angle of 19.5°, 91.8% of the scattered neutron beam is transmitted through the detecting scintillator. At 25°, 91.1% go through. Since the attenuation depends on the energy of the neutrons incident on the detecting scintillator,

corrections to the differential cross section of 0.5% at 19.5° and 1.3% at 25° result.

D. Attenuation in Target and Air

The actual neutron flux in the detecting scintillator differed from that measured at 0° because of the exponential attenuation of the neutron beam as it passed through the target. Five separate factors must be taken into account in the calculation of this effect:

(1) The exponential attenuation of the neutron beam entering the target scintillator must be included. This will decrease the average beam intensity passing through the target. This correction was calculated by partitioning the target scintillator into 15 segments and calculating the transmission (T_i) through half the thickness of each segment.

(2) The effect of exponential attenuation of the neutron beam coming out of the target towards the detector must be included. Here we must consider both the decrease in the flux density directed towards the detector by outscattering and the increase in this flux density by neutrons which scatter first in some other direction and then towards the detector (inscattering). This calculation has been done more accurately in the multiple scattering program but is included here because it is also needed in the calculation of the average scattering angle.

(3) The effect of exponential attenuation by the material (glass, tape and aluminum foil) surrounding the scintillator fluid must also be included. This must be considered for both incident and outgoing neutron beams. This correction was calculated from the experimentally observed transmission through the scintillator (including container, etc.)

and the calculated transmission through the scintillator fluid alone. This was a 3.9% correction to the differential cross section.

(4) The effect of differing distances and scattering angles at different locations in the target scintillator must also be included.

(5) Exponential attenuation by the air must be taken into account. This applies to both the 0° measurement of the direct flux density and the measurement of the scattered flux density. The effect will be greater at 0° than at the scattering angle θ since the distance from the neutron source to the detector is greater at 0°. The net correction to the cross section is -0.1%.

The target scintillator was partitioned into 15 segments (5 in the horizontal plane by 3 in the vertical plane) to calculate and measure the effects 1, 2 and 4 above.

The differential cross section (Eq. 1) may be rewritten as[10]

$$\overline{\sigma(\theta)} = (1+\delta)\,\sigma(\theta), \tag{3}$$

where

$$1 + \delta = \left\{ \sum_{i=1}^{15} \frac{C_i}{C_8}\, T_i T'_i\, \frac{Vi}{V} \left(\frac{d_8}{d_i}\right)^2 \right\}^{-1}, \tag{4}$$

and

C_i is the measured neutron flux in the i^{th} segment (8 denotes the middle position, the position at which all 0° flux measurements were made),

T_i is the transmission of the incoming neutron beam through half the thickness of the i^{th} segment of the scintillator fluid,

T_i' is the transmission of the outgoing neutron beam through

the remaining thickness of scintillator fluid towards the target. T_i' was set equal to 1 to calculate δ because this effect is already included in the multiple scattering correction. It was needed for the average scattering angle calculation,

V_i is the volume of the i^{th} segment, V is the total volume, and d_i is the distance from the center of the i^{th} segment to the detecting scintillator.

At a scattering angle of 19.5°, δ is 0.077; at 25.1°, δ is 0.076.

Average scattering angles were calculated from these parameters using the equation

$$\bar{\theta} = \frac{\sum_{i=1}^{15} \theta_i V_i \frac{C_i}{C_8} \frac{1}{d_i^2} T_i T_i'}{\sum_{i=1}^{15} V_i \frac{C_i}{C_8} \frac{1}{d_i^2} T_i T_i'} . \qquad (5)$$

A geometrical θ of 19.46° corresponded to $\bar{\theta}$ = 19.53°, and a geometrical θ of 25.09° became 25.13°.

E. Wall Effects

The range of a 24-MeV proton recoiling from a head-on collision with a 24-MeV neutron is 0.67 cm in toluene, the liquid of the scintillator. The diameter of the scintillator is 2.54 cm. Consequently, many of the recoils in the detector do not have their full range inside the scintillator, and their observed light output corresponds to

an energy less than their actual energy.

A Monte-Carlo routine calculated this effect. The program traced the paths of some 2×10^5 neutrons of each incident energy through the scintillator. All incident neutrons interacted with the scintillator and appropriately weighted random numbers were chosen for all scattering parameters.

Since this wall effect occurs both when the detector is at 0° for an incident flux density measurement and at the scattering angle θ, the ratio of the effects in both places will give the correction to the differential cross section. At a bias of $0.5\ E_0$, the correction to the differential cross section is -2% at 19.5° and -3.3% at 25.1°.

Wall effects in the target scintillator must also be included. If a neutron is to meet all the electronic requirements for scattering from a proton in the target into the detecting scintillator, it must produce a detectable recoil proton in the target scintillator. A lower level discriminator threshold was set on pulses coming from the target scintillator. If a recoil proton is produced so close to the wall of the target scintillator that part of its range lies outside the scintillator, this recoil will be lost if the observed pulse height is less than the discriminator threshold. This wall effect is simple to calculate because the geometry involved is well determined. In order for the scattered neutron to hit the detecting scintillator the scattering must take place in or near the horizontal plane and all recoils must go in approximately the same direction. Let the minimum detectable pathlength be ε. The number of recoils which are not detected because they occur too close to the wall is then proportional to the non-overlapping area of two circles with

their centers separated by a distance ε. The fraction of recoils occurring in this area is given by[10]

$$f_m = 1 - \frac{2}{\pi} \cos^{-1} \left(\frac{\varepsilon}{2r}\right) + \frac{\varepsilon}{\pi r} \left(1 - \frac{\varepsilon^2}{4r^2}\right)^{1/2} \qquad (6)$$

where r is the scintillator radius. The calculation is exact for any value of ε.

At 19.5°, the minimum detectable recoil energy was 1.4 MeV. This corresponds to an ε of 0.0046 cm (from Janni[12]) and a correction to the differential cross section of +0.2%. At 25°, the minimum detectable recoil energy was 2.25 MeV corresponding to an ε of 0.010 cm and a correction to the differential cross section of +0.5%.

5. RESULTS

A. Measured Cross Sections

Table II presents the measured differential cross sections at an average scattering angle of 25.1°(lab) as a function of bias energy. The values quoted are in the lab and uncorrected. Corrections are given in Section 5B. The errors given in this table are statistical only. Data sets I-III differ in the tritium pressure of the gas cell used for the neutron source. The overall average is weighted by the statistical error of each data set. Lower bias levels are excluded because the $D(d,n)^3He$ and $^{12}C(n,n')3\alpha$ reactions enter.

Figure 5a is a histogram of all the differential cross section measurements at 25°. Each square represents a measurement of the differential cross section within the indicated 2 mb/sr interval. Statistical errors on each point are about 5%. The spread in the data points

about the average values (indicated on the histograms by the dashed lines) was used to obtain standard errors.

Table III presents the measured differential cross sections at an average lab scattering angle of 19.5°. The cross section values are in the lab system and uncorrected, and the errors quoted in this table are statistical only. Data sets 1-6 differ in the electronics used and in the tritium pressure in the neutron source.

Figure 5b is a histogram of the differential cross section measurements at 19.5° as a function of bias energy. Statistical errors on each point are approximately 5%. No distinction is made between data from neutrons scattered to the left and to the right in the lab in these histograms because no statistically significant differences were found between left and right scattering. The dashed lines again indicate the average values, and the spread in the data about this value was used to obtain a standard error.

B. Corrections to the Cross Section Data

Table IV presents the corrections to the data. The uncertainty in the differential cross section due to these corrections is approximately 1.5%, and is principally due to uncertainties in the exponential attenuation correction δ, the multiple scattering correction, and uncertainties in the differential cross section itself which results in errors in the bias factor f_B (see below).

Table V presents the corrected c.m. cross sections and the corrected c.m. angles at which they were observed. The average values are obtained by averaging data at each bias. Since the data sets are

correlated, this averaging does not improve the statistical accuracy.

C. Error Analysis

Table VI lists the errors in the cross section measurement.

The standard error was estimated by taking sums of squares of deviations from the mean cross section at each bias energy and dividing by N(N-1) where N is the number of observations. 16 separate measurements were made of the differential cross section at 25°, 50 at 19.5°.

The error in δ was estimated by observing the changes that occurred in the calculated value of δ with extreme variation of the input parameters. It includes errors for target exponential attenuation corrections.

The error in f_B was estimated by assuming that the bias was known to 1% and calculating the uncertainty in f_B as a function of the scattering angle θ. This corresponds to an uncertainty of approximately 4 channels in the estimate of the maximum recoil proton energy in the direct neutron beam.

The error in n_p is the error quoted by Galbraith Labs in their analysis of the hydrogen and carbon content of the scintillator fluid.

The error in the correction for the finite range of the recoil protons is the statistical error based on the number of neutron trajectories traced by the Monte-Carlo calculation.

The multiple-scattering error is the statistical error based on the number of neutron trajectories followed by the Monte-Carlo multiple scattering program.

The column labeled 'RMS Error' is the RMS sum of all the errors

quoted in the table except those due to counting statistics. The final column is the RMS sum of all errors.

6. CONCLUSIONS

The cross section measured at 19.5°(lab) or 39.3°(c.m.) is 31.3±0.5 mb/sr. The cross section calculated from the LRL phase shifts by Hopkins and Breit[3] is 31.3 mb/sr. The value they calculate from the Yale phase shifts is 31.0 mb/sr.

The cross section measured at 25.1°(lab) or 50.5°(c.m.) is 30.7±0.6 mb/sr. The cross section calculated from the LRL phase shifts by Hopkins and Breit is 31.0 mb/sr. The value they calculate from the Yale phase shifts is 30.7 mb/sr.

Figure 6 is a plot of all the available 24 MeV data.[4,5] All measurements were carried out at Wisconsin using two different experimental techniques. Also plotted on the graph for comparison are a symmetric Gammel curve, and both the LRL and Yale phase shift calculations from Hopkins and Breit. No attempt has been made here to make an additional fit to the data. The data confirm the expected fore-aft asymmetry and indicate that the Hopkins and Breit predictions are impressively good.

REFERENCES

† Now at Hahn-Meitner-Institut, Kernphysik, Berlin, W. Germany

†† Work supported in part by the U.S. Atomic Energy Commission

1 J.L. Gammel in Fast Neutron Physics, Part II, edited by J.B. Marion and J.L. Fowler (Interscience Publishers, Inc., New York, 1963), p 2185.

2 J.P. Scanlon, G.H. Stafford, J.J. Thresher, P.H. Bowen and A. Langsford, Nucl. Phys. 41, 401 (1963).

3 J.C. Hopkins and G. Breit, Nucl. Data A9, 137 (1971).

4 L.N. Rothenberg, Phys. Rev. C1, 1226 (1970).

5 T.W. Burrows, Bull. Am. Phys. Soc. 17, 151 (1972) and Thesis, University of Wisconsin, 1972 (unpublished).

6 T.G. Masterson, Nucl. Instr. and Meth. 88, 61 (1970).

7 Supplied by Nuclear Enterprises, Inc., San Carlos, Calif. The mass of the target scintillator fluid was also measured by this firm.

8 Determined by Galbraith Laboratories, Knoxville, Tenn.

9 J.B. Marion and F.C. Young, Nuclear Reaction Analysis (North Holland Publishing Co., Amsterdam, 1968), p. 116.

10 T.G. Masterson, Thesis, University of Wisconsin, 1971 (unpublished).

11 R.E. Phillips and S.T. Thornton, A FORTRAN Program for Relativistic Calculations in Two-Body Nuclear Reactions, ORNL Report 4179 (1967).

12 J.F. Janni, Calculations of Energy Loss, Range, Pathlength, Straggling, Multiple Scattering, and the Probability of Inelastic Nuclear Collisions for 0.1 to 1000-MeV Protons, Technical Report No. AFWL-TR-65-150 (1966).

FIGURE CAPTIONS

Fig. 1 (a) Geometry for 0° flux measurement

(b) Scattering geometry

(c) Detail of tritium gas cell

Fig. 2 (a) Simplified block diagram of electronics

(b) Electronics used in data collection

① = recoil proton spectra gated by "real' neutrons ③ or 'accidental' neutrons ⑤

② = TAC spectra gated by 'real' neutrons ④ or 'accidental' neutrons ⑥

⑦ = fast linear spectrum from target scintillator gated by TOF and n-γ requirements

⑧ = n-γ spectrum

Fig. 3 (a) Recoil proton spectra observed in the 0° neutron beam

(b) Recoil proton spectrum observed at a scattering angle of 25.1°. The numbers above the arrows indicate biases expressed as a fraction of the incident neutron energy. Their value includes the effect of the non-linear response of the scintillator

(c) Recoil proton spectrum observed at a scattering angle of 19.5°

Fig. 4 Time-of-flight spectra for neutrons scattered from the target scintillator into the detecting scintillator. FWHM is approximately 2 ns.

Fig. 5 (a) Histogram of 25.1° data as a function of bias energy

(b) Histogram of 19.5° data as a function of bias energy. Each block represents a differential cross section measurement within the indicated 2 mb/sr interval

Fig. 6 Wisconsin n-p differential cross section measurements. Only the present results are absolute determinations.

TABLE I

Effect of different angular distributions on bias factors

Bias (B/E_0)	Ratio of bias factors $f_B(E_0)/f_B(E_1)$ for angular distributions		
	Isotropic	Gammel	Hopkins
	E_0 = 24 MeV, E_1 = 21.35 MeV		
0.45	1.113	1.110	1.115
0.5	1.142	1.137	1.146
0.55	1.179	1.172	1.186
	E_0 = 24 MeV, E_1 = 19.69 MeV		
0.45	1.219	1.208	1.217
0.5	1.281	1.265	1.282
0.55	1.366	1.345	1.372

TABLE II

Laboratory differential cross sections measured at 25.1°

No corrections are included in these values other than those contained in the data analysis program

Data Set	Bias = 0.45		Bias = 0.5		Bias = 0.55	
	σ (mb/sr)	Δσ (%)	σ (mb/sr)	Δσ (%)	σ (mb/sr)	Δσ (%)
I	98.2	1.9	99.4	2.1	100.4	2.2
II	98.4	1.7	100.4	2.0	100.4	2.2
III	98.4	1.6	99.7	1.7	100.1	1.9
Average	98.3	1.0	99.8	1.1	100.3	1.2

TABLE III

Laboratory differential cross sections measured at 19.5°

No corrections are included in these values other than those contained in the data analysis program

Data Set	Bias = 0.45		Bias = 0.50		Bias = 0.55	
	σ (mb/sr)	Δσ (%)	σ (mb/sr)	Δσ (%)	σ (mb/sr)	Δσ (%)
1	102.8	1.3	103.0	1.4	101.9	1.5
2	103.2	1.6	103.8	1.7	103.4	1.9
3	102.3	1.3	102.2	1.4	101.1	1.5
4	100.1	1.3	100.0	1.4	98.2	1.6
5	106.7	1.6	108.7	1.7	109.0	1.8
6	106.0	1.4	105.6	1.5	104.7	1.6
Average	103.3	0.6	103.6	0.6	102.7	0.7

TABLE IV

Corrections

All corrections are given in percent

θ_{lab} (°)	Bias B/E_0	Attenuation 1	2	3	4	5	6	7	8	9	Total
19.5	0.45	7.7	3.9	-0.1	-0.3	-0.1	5.8	0.5	0.2	-1.8	15.7
	0.50									-2.0	15.5
	0.55									-2.3	15.3
25.1	0.45	7.6	3.9	-0.1	-0.3	-0.1	3.4	1.3	0.5	-2.9	13.3
	0.50									-3.3	12.9
	0.55									-3.7	12.5

1. Exponential attenuation of the neutron beam by the target scintillator fluid
2. Exponential attenuation of the neutron beam by the container of the target scintillator fluid
3. Exponential attenuation of the neutron beam by air
4. Effect of finite length of neutron source
5. Effect of finite length of target
6. Multiple scattering correction
7. Effect of finite detector thickness -- exponential attenuation of neutron beam in detector
8. Effect of finite range of recoil protons in target
9. Effect of finite range of recoil protons in detector

TABLE V

Summary of cross-section measurements and corrections

θ_{lab}	Bias (B/E_0)	σ_{lab} uncorrected mb/sr)	Correction (percent)	c.m. Conversion factor	$\sigma_{c.m.}$ (mb/sr)	$\theta_{c.m.}$
	0.45	103.3	15.7		31.4	
19.5°	0.50	103.6	15.5	0.262	31.4	39.3°
	0.55	102.7	15.3		31.1	
	0.45	98.3	13.3		30.5	
25.1°	0.50	99.8	12.9	0.273	30.8	50.5°
	0.55	100.3	12.5		30.8	

$\overline{\sigma}(39.3°) = 31.3 \pm 0.5$ mb/sr

$\overline{\sigma}(50.5°) = 30.7 \pm 0.6$ mb/sr

TABLE VI

Errors

All values are given in percent

θ (lab)	Bias (B/E_0)	Counting statistics	Standard error	δ	f_B	n_p	Finite range of recoil protons	Multiple scattering	RMS error without counting statistics	Overall error
	0.45	0.6	0.7						1.3	1.4
19.5°	0.50	0.6	0.7	0.5	0.7	0.4	0.2	0.6	1.3	1.4
	0.55	0.7	0.7						1.3	1.5
	0.45	1.0	1.0						1.7	2.0
25.1°	0.50	1.1	1.1	0.6	1.1	0.4	0.3	0.6	1.8	2.1
	0.55	1.2	1.1						1.8	2.2

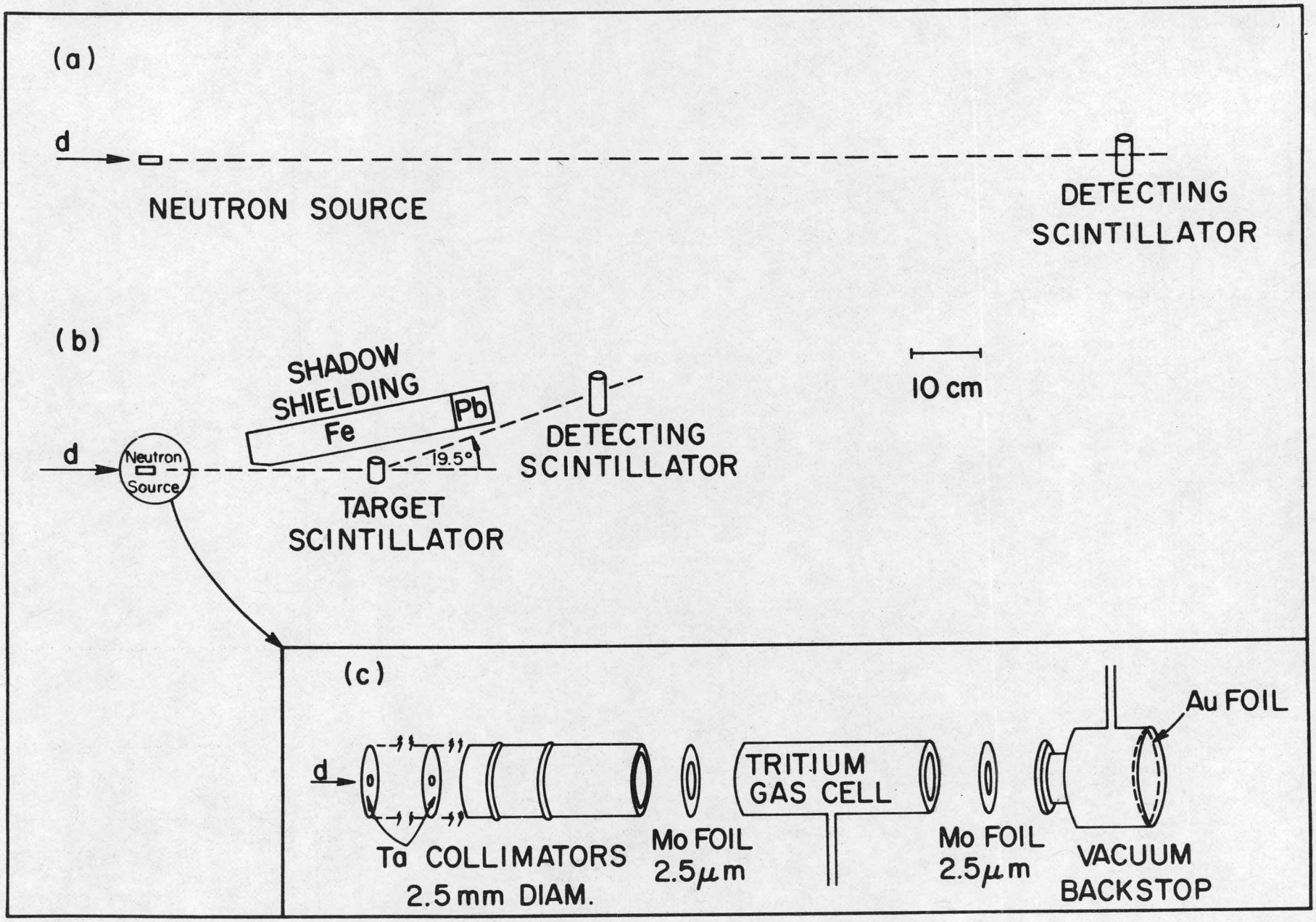
(a)
d
NEUTRON SOURCE
DETECTING SCINTILLATOR
(b)
SHADOW SHIELDING
Fe
Pb
19.5°
d
Neutron Source
TARGET SCINTILLATOR
DETECTING SCINTILLATOR
10 cm
(c)
d
Ta COLLIMATORS 2.5 mm DIAM.
Mo FOIL 2.5μm
TRITIUM GAS CELL
Mo FOIL 2.5μm
Au FOIL
VACUUM BACKSTOP

Fig. 1

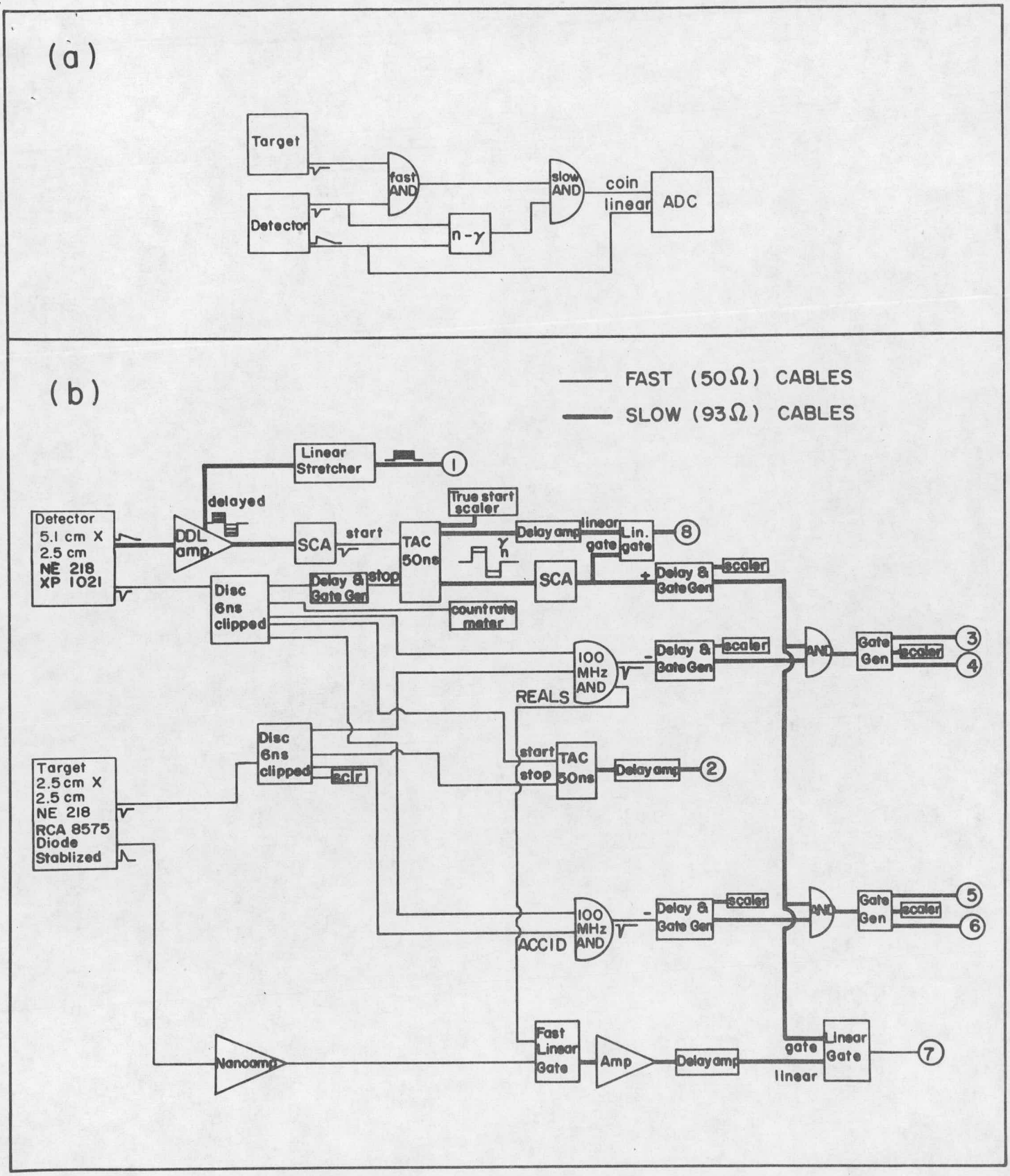
(a)
Target
Detector
fast AND
n-γ
slow AND
coin
linear
ADC
(b)
FAST (50Ω) CABLES
SLOW (93Ω) CABLES
Linear Stretcher
delayed
Detector 5.1 cm X 2.5 cm NE 218 XP 1021
DDL amp.
SCA
start
TAC 50ns
True start scaler
Delay amp
linear gate
Lin. gate
γ n
SCA
Delay & Gate Gen
scaler
Disc 6ns clipped
Delay & Gate Gen
stop
count rate meter
100 MHz AND
REALS
Delay & Gate Gen
scaler
AND
Gate Gen
scaler
Disc 6ns clipped
scir
start
stop
TAC 50ns
Delay amp
Target 2.5 cm X 2.5 cm NE 218 RCA 8575 Diode Stablized
100 MHz AND
ACCID
Delay & Gate Gen
scaler
AND
Gate Gen
scaler
Nanoamp
Fast Linear Gate
Amp
Delay amp
gate
linear
Linear Gate

Firue 2

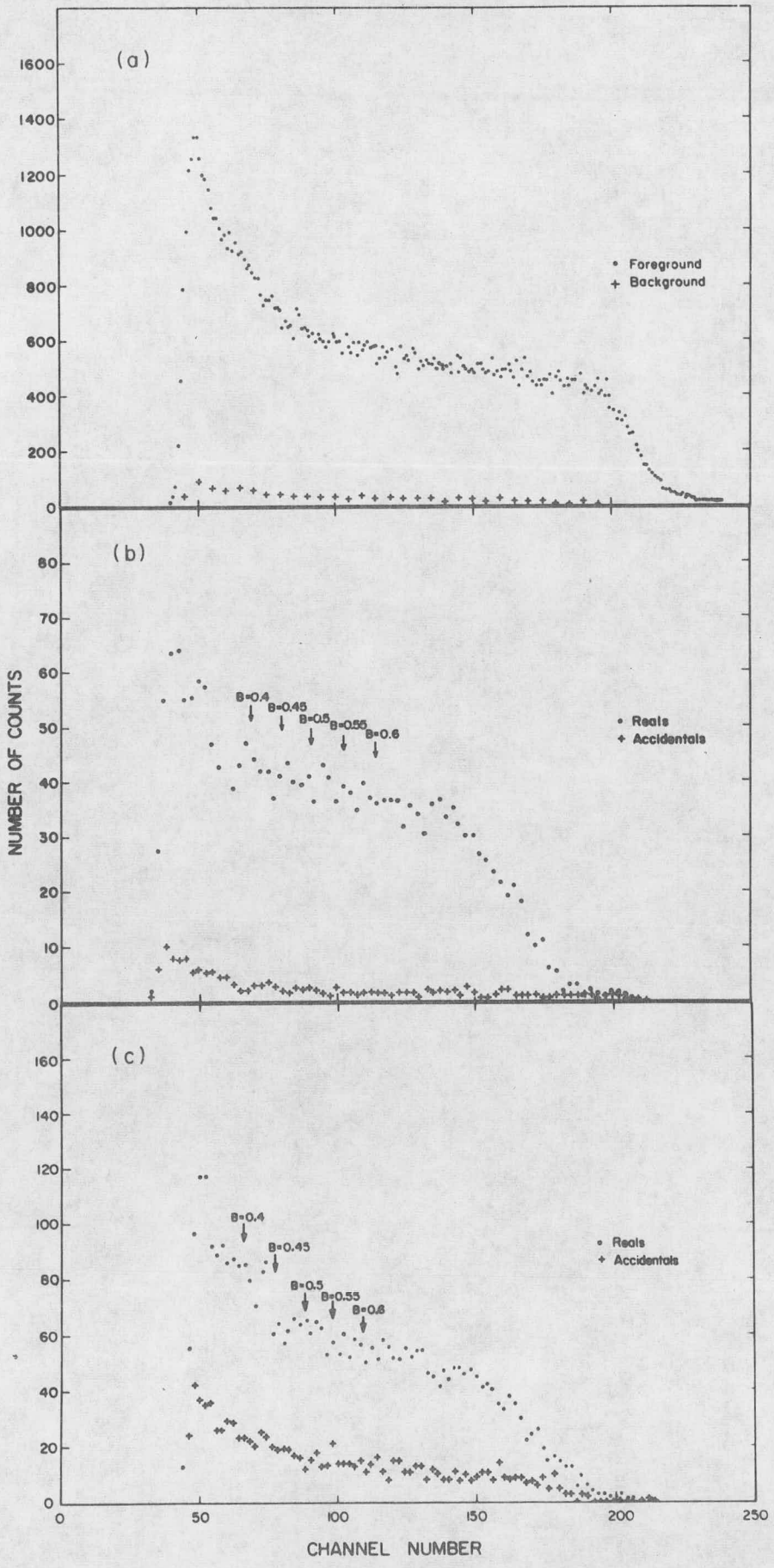
(a)
Foreground
Background
(b)
B=0.4
B=0.45
B=0.5
B=0.55
B=0.6
Reals
Accidentals
(c)
B=0.4
B=0.45
B=0.5
B=0.55
B=0.6
Reals
Accidentals
NUMBER OF COUNTS
CHANNEL NUMBER

Figure 3

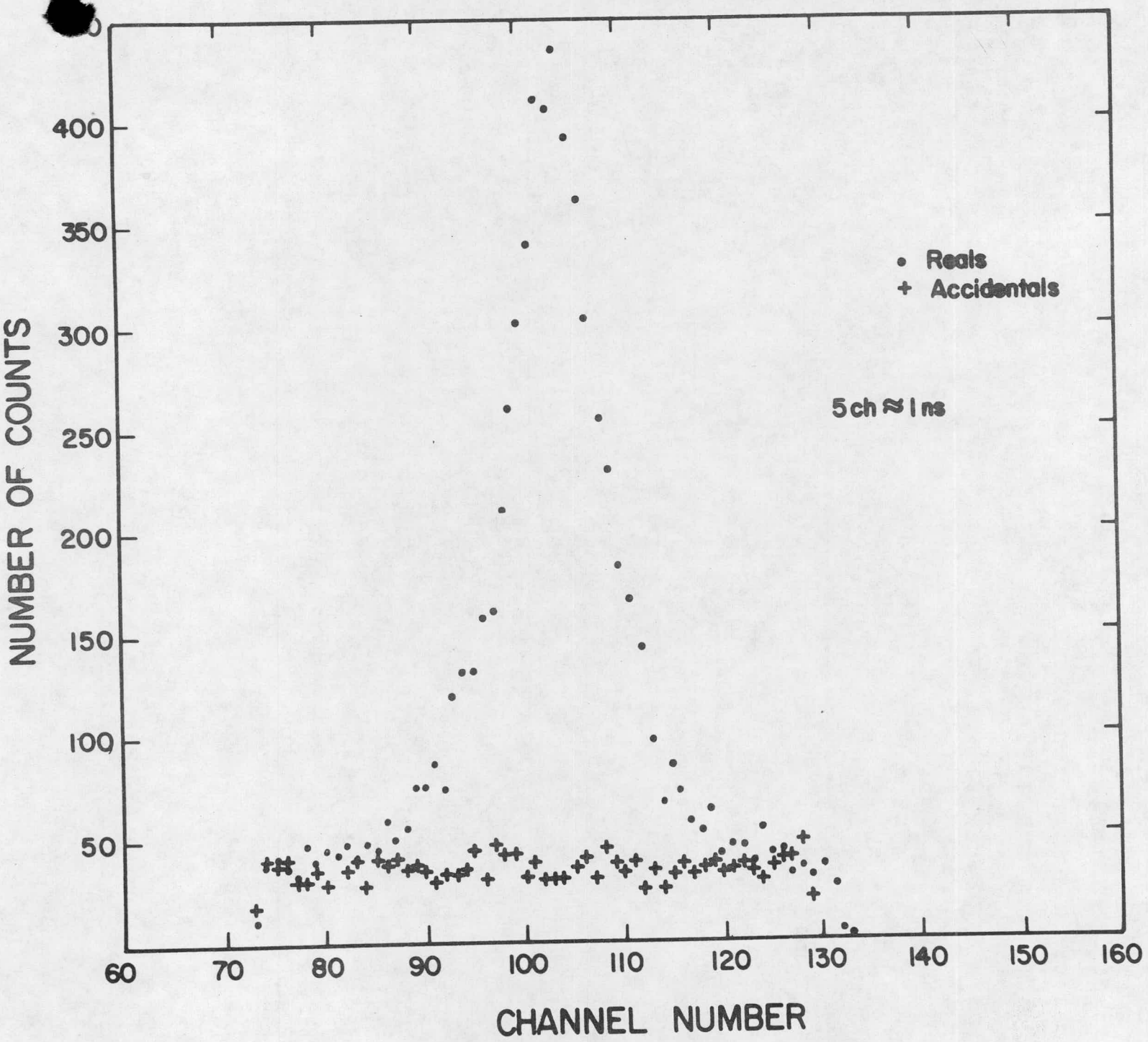
NUMBER OF COUNTS
400
350
300
250
200
150
100
50
60
70
80
90
100
110
120
130
140
150
160
CHANNEL NUMBER
• Reals
+ Accidentals
5ch ≈ 1ns

Firure 4

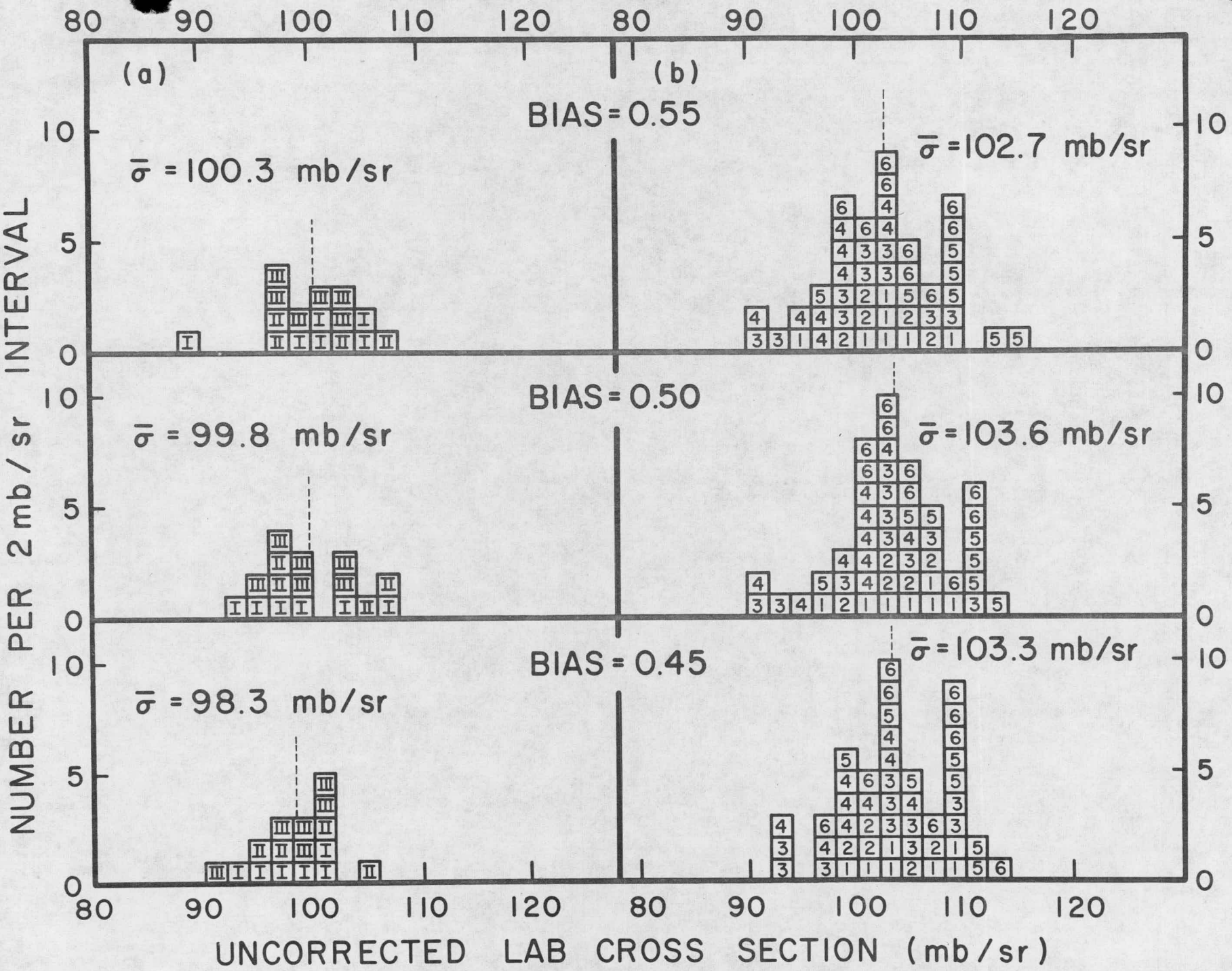
(a)
(b)
BIAS = 0.55
$\bar{\sigma}$ = 100.3 mb/sr
$\bar{\sigma}$ = 102.7 mb/sr
BIAS = 0.50
$\bar{\sigma}$ = 99.8 mb/sr
$\bar{\sigma}$ = 103.6 mb/sr
BIAS = 0.45
$\bar{\sigma}$ = 98.3 mb/sr
$\bar{\sigma}$ = 103.3 mb/sr
NUMBER PER 2 mb/sr INTERVAL
UNCORRECTED LAB CROSS SECTION (mb/sr)
80
90
100
110
120
0
5
10

Figure 5

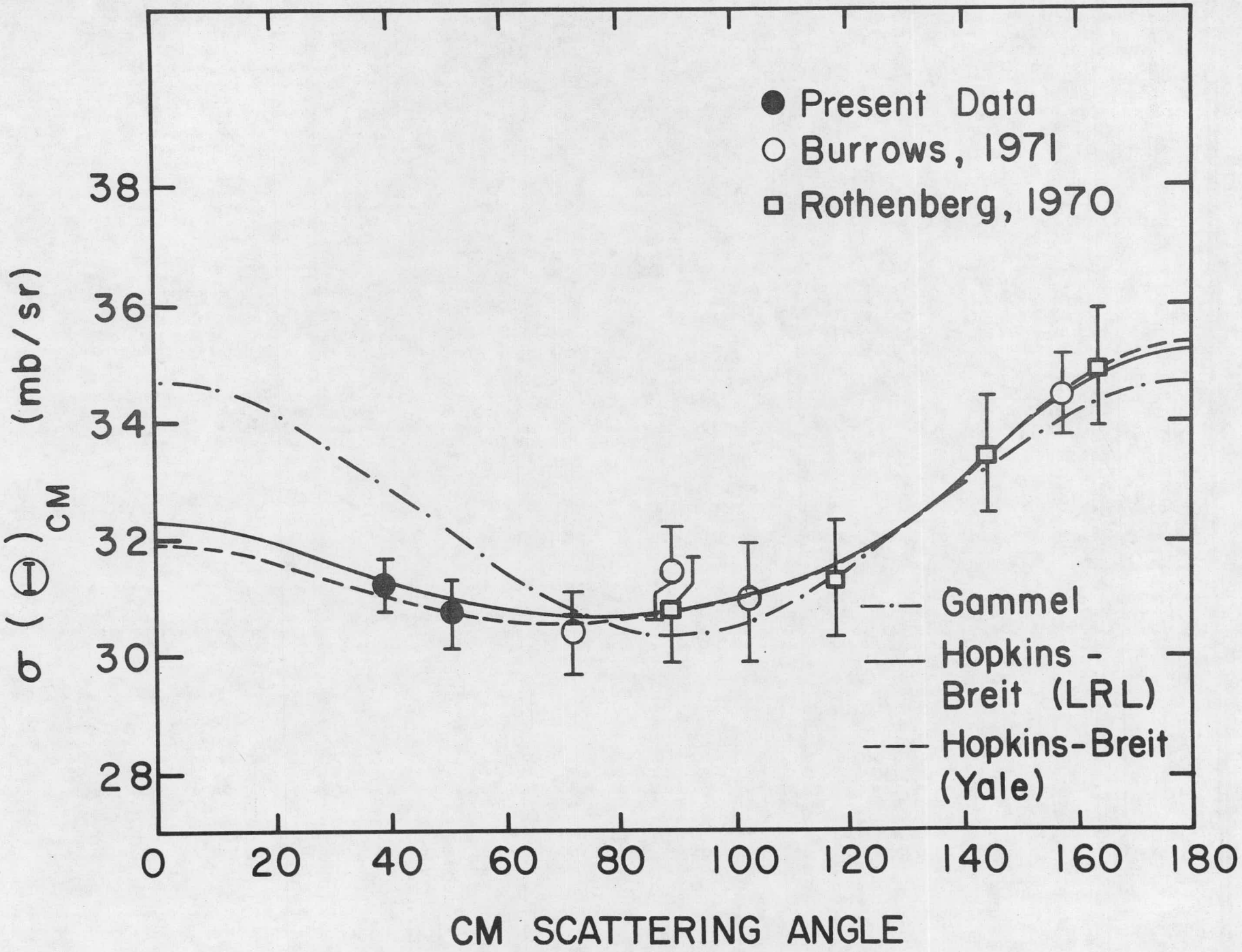
● Present Data
○ Burrows, 1971
□ Rothenberg, 1970
38
36
34
32
30
28
σ (Θ)CM (mb/sr)
Gammel
Hopkins - Breit (LRL)
Hopkins-Breit (Yale)
0
20
40
60
80
100
120
140
160
180
CM SCATTERING ANGLE

Figure 6